Coded Excitation for Increased Sensitivity in Transcranial Power Doppler Imaging

Emelina Vienneau, Abbie Weeks, and Brett Byram
Department of Biomedical Engineering
Vanderbilt University
Nashville, TN, USA
emelina.p.vienneau@vanderbilt.edu

2022 IEEE International Ultrasonics Symposium (IUS) | 978-1-6654-6657-8/22/$31.00 ©2022 IEEE | DOI: 10.1109/IUS54386.2022.9958842

***Abstract*—Functional ultrasound imaging (fUSI) is a promising new modality for neuroimaging that measures the power Doppler signal as a proxy for neural activation. However, clinical translation of noninvasive, transcranial fUSI (tfUSI) is hindered by the low signal-to-noise ratio (SNR) from the skull which greatly limits blood flow sensitivity. To overcome this issue, we demonstrate a coded excitation approach to increase SNR in transcranial power Doppler imaging and thereby increase blood flow sensitivity. In three healthy adult subjects we showed an average SNR gain of 17.77 $\pm$ 1.05 dB, contrast-to-noise ratio gain of 4.97 $\pm$ 4.18 dB, and contrast ratio gain of 22.53 $\pm$ 11.34 dB using a 65 bit code. These promising results indicate that tfUSI may be feasible using our coded excitation approach.**

***Index Terms*—Coded excitation, transcranial ultrasound imaging, power Doppler imaging**

I. Introduction

Functional ultrasound imaging (fUSI) is an emerging neuroimaging modality that measures blood flow in the brain as a proxy for neural activation. fUSI measures the power Doppler signal which is linearly proportional to cerebral blood volume, an important component of the hemodynamic response [1]. fUSI has shown great promise as a neuroimaging modality in invasive animals models as well as a few niche clinical applications in which the skull can by bypassed such as transfontanellar imaging in neonates and imaging through a craniotomy during neurosurgery [2]–[5].

However, clinical translation of noninvasive, transcranial fUSI (tfUSI) remains unsolved due to low signal-to-noise ratio (SNR) from the skull. The structural inhomogeneities of the skull as well as its high acoustic impedance mismatch with the surrounding tissue leads to several sources of image degradation including attenuation, reverberation, and phase aberration which contribute to low SNR [6]. Furthermore, since attenuation is frequency dependent, low frequencies (1-4 MHz) are needed to penetrate the skull. Lower transmit frequencies lead to lower scattering by blood and also increase the minimum detectable velocity, both of which lead to limited blood flow sensitivity [7]–[9]. Advanced post-processing methods such as adaptive demodulation and singular value decomposition (SVD) can improve the separability between tissue, blood, and noise and therefore improve visualization of slower flow, but these methods also perform better with higher SNR [10], [11]. In summary, higher SNR is needed to overcome the limitations of the skull and make tfUSI possible in non-neonates.

One approach to increasing SNR in transcranial blood flow imaging is to use microbubble contrast agents [12]. However, microbubble localization techniques require long scan times on the order of tens of seconds or minutes, making it difficult to measure transient hemodynamic fluctuations due to the neural activity. Moreover, using microbubbles requires perfectly timed and calibrated injections to ensure the concentration in the blood stream is consistent and known over time. This increases the complexity (and invasiveness) of the imaging procedure and ultimately renders it impractical for many clinical applications.

Coded excitation is an alternative approach that could be used to improve SNR in transcranial blood flow imaging without relying on contrast agents. Coded excitation is a signal processing technique in which modulated excitation waveforms are used to safely increase the power transmitted into the tissue within FDA safety limits. The received data is then demodulated to recover the original axial resolution and create an SNR gain [13], [14]. We have previously presented a coded excitation technique designed to generate large SNR gains without sacrificing frame rate or other aspects of image quality [15]–[17]. Our approach uses compound Barker codes to create arbitrarily long coded excitation waveforms which provide large SNR gains proportional to $10\log_{10}(N)$. To perform pulse compression without introducing range lobe artifacts, we use inverse filtering instead of matched filtering which is possible due to the mathematical properties of the compound Barker codes. In this work, we applied this coded excitation framework in transcranial power Doppler imaging of three healthy adult volunteers to assess how the SNR gain from coded excitation can generate sensitivity improvements in blood flow imaging.

The work of Emelina P. Vienneau was supported in part by the National Science Foundation Graduate Research Fellowship Program under Grant 1937963 and in part by the National Institute of Biomedical Imaging and Bioengineering under NIH Grant T32EB021937. The work of Brett C. Byram was supported in part by the National Institute of Biomedical Imaging and Bioengineering under NIH Grant R01EB020040; in part by the National Heart, Lung, and Blood Institute under Grant R01HL156034; and in part by the National Science Foundation CAREER Award under Grant IIS-1750994.

II. Methods

A. Coded Excitation Framework

1) Formation of the Coded Excitation Waveform: The first step in coded excitation ultrasound imaging is to generate the coded excitation waveform. The coded excitation waveform is created by modulating the transmit waveform to make it longer in order to safely transmit more power into the tissue and create an SNR gain. This is achieved by convolving a base pulse, referred to as the encoding chip pulse, with a binary code, generating an SNR gain proportional to $10\log_{10}(N)$, where N is the length of the binary code. The encoding chip is a standard transmit waveform that defines the axial resolution of the system (*e.g.*, a single-cycle sine wave at the center frequency of the transducer). Convolving the chip pulse with an upsampled binary code creates a phase modulated excitation waveform where the positive bits correspond to a 0° phase shift and the negative bits correspond to a 180° phase shift. Importantly, the binary code is upsampled by a factor equal to the length of the encoding chip before convolution.

In order to generate large SNR gains, long binary codes are needed. We have shown that arbitrarily long invertible binary codes can be formed by taking the Kronecker product of shorter invertible codes such as Barker codes [15]–[17]. For this work, we tested a 13 bit Barker code, a 39 bit compound Barker code (formed by combining the 3 bit and 13 bit Baker codes), and a 65 bit compound Barker code (formed by combining the 5 bit and 13 bit Barker codes). Importantly, the binary code must be invertible, meaning it has no zeros in the Fourier domain, in order to use an inverse filtering approach for pulse compression.

2) Formation of the Decoding Filter for Pulse Compression: The next step is to create the decoding filter which is used to perform pulse compression of the received data. In order to perform pulse compression without introducing range lobe artifacts, we used inverse filtering instead of matched filtering which is possible since the binary codes are invertible. To construct the L-tap finite impulse response (FIR) decoding filter, the discrete Fourier transform of the binary code is first computed. The resulting spectrum is inverted and then first L samples of the inverse discrete Fourier transform are computed. Finally, the filter is upsampled by the length of the encoding chip waveform and convolved with the decoding chip waveform. The decoding chip waveform is the two-way impulse response of the imaging system. For more details on the construction of the decoding filter, see Refs. [15]–[17]. To perform pulse compression, the decoding filter is convolved with the received channel data along the axial dimension.

B. In Vivo Transcranial Power Doppler Imaging

A P4-2v phased array transducer ($f_0 = 2.7174$ MHz, pitch = 300 μm) and a Verasonics Vantage 128 scanner (Kirkland, WA, USA) were used for *in vivo* imaging. The derated ISPPA was matched for all transmit waveforms and the acoustic output was measured with a hydrophone to ensure it was within the FDA safety limits for diagnostic imaging [18]. All imaging was done according to a protocol approved by the local IRB. Imaging was performed in the transverse plane at the right temporal acoustic window with a hand-held transducer. Three healthy adult volunteers were recruited (two males and one female; age range 23-26; all Caucasian).

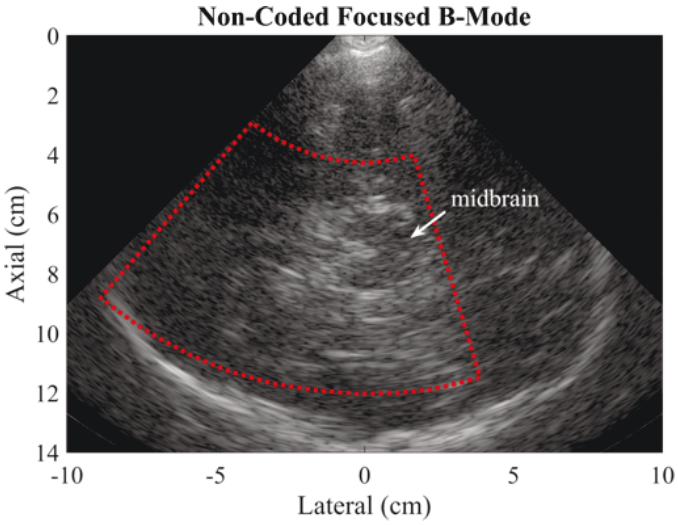

Fig. 1. Focused B-Mode acquired for real-time guidance in Subject 3. The red dotted box indicates the ROI used for power Doppler processing. The midbrain structure is also indicated with the arrow. Image shown on a 70 dB dynamic range.

Data was acquired with code lengths of 13 bits, 39 bits, and 65 bits using a 21 V transmit voltage. For each code length, coded and non-coded excitation datasets were acquired sequentially with matched field-of-views (FOVs). The non-coded excitation pulse (and the encoding chip for the coded excitation pulses) was a single-cycle parametrically defined pulse at a center frequency of 2.7174 MHz. The decoding filter for pulse compression was a 256-tap FIR filter.

Blood flow imaging was performed with a diverging wave synthetic aperture (DWSA) power Doppler sequence to simultaneously optimize for a high frame rate acquisition while obtaining a wide field-of-view. The DWSA sequence consisted of 8 diverging wave transmits with 15 element sub-apertures spaced evenly across the aperture. There were 1100 total acquisitions with a 550 Hz frame rate. For beamforming, a sector geometry with a 90° opening angle and a radius of 9.6 mm was chosen and 128 evenly spaced beams were beamformed using dynamic receive. Clutter filtering was performed on 100-sample ensembles. Two clutter filtering approaches were tested: a simple high-pass filter and SVD [11]. With the SVD approach, only clutter was removed (not noise) in order to better observe the effects of coded excitation on the noise floor of the image. The high pass filter was a 6^{th} order Chebyshev infinite impulse response (IIR) filter with a 10 Hz cutoff frequency. Since the non-coded and coded excitation images were acquired sequentially and therefore at different points in the cardiac cycle, the best and most highly similar 100-sample ensembles were chosen for each coded and non-coded excitation pair. Since blood flow was not visible in the

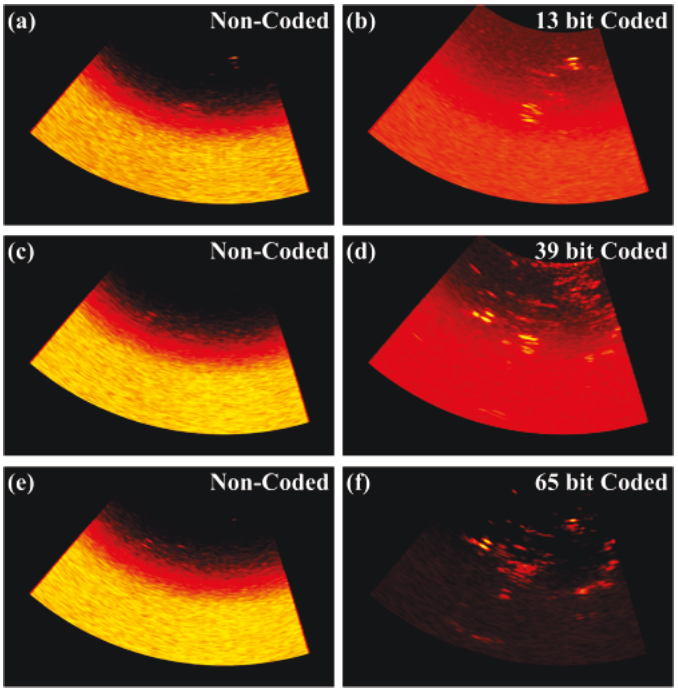

Fig. 2. Transcranial power Doppler in Subject 3 with clutter filtering performed via a high pass IIR filter. Non-coded excitation images are shown on a 10 dB dynamic range on the left in panels **(a)**, **(c)**, and **(e)**. Their respective coded excitation pairs are shown on the right on a 25 dB dynamic range in panels **(b)**, **(d)**, and **(f)** which correspond to code lengths of 13, 39, and 65, respectively.

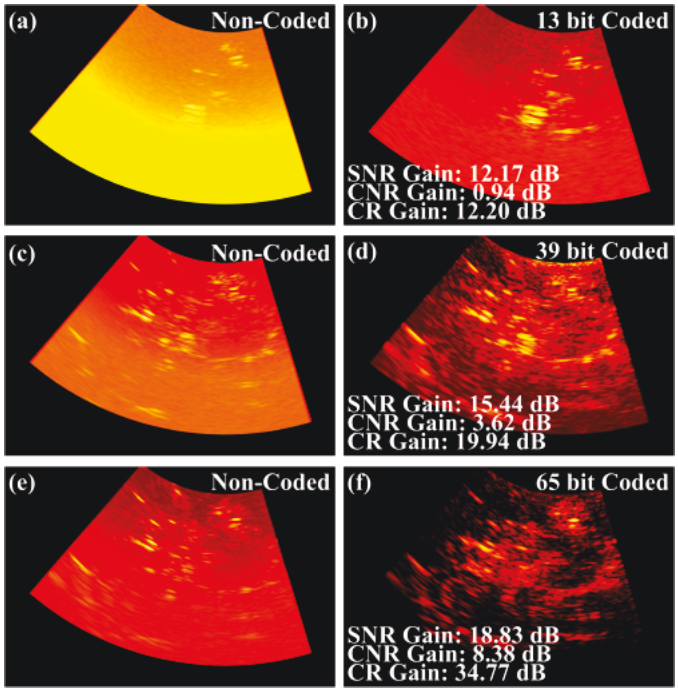

Fig. 3. Transcranial power Doppler in Subject 3 with clutter filtering performed via SVD. Non-coded excitation images are shown on the left in panels **(a)**, **(c)**, and **(e)**. Their respective coded excitation pairs are shown on the right in panels **(b)**, **(d)**, and **(f)** which correspond to code lengths of 13, 39, and 65, respectively. The coded excitation panels also have the SNR gain, CNR gain, and CR gain indicated in the bottom left corner. All images are shown on the same 40 dB dynamic range.

non-coded IIR filtered data, the ensembles were chosen based on the SVD filtered data where blood flow was more visible.

Finally, focused M-Mode with and without coded excitation was also performed with each acquisition in order to provide high pulse repetition frequency (PRF) data to calculate SNR in the presence of physiological and sonographer motion. The focused M-Mode sequence acquired 2000 frames with a steering angle of 0°, a PRF of 1 kHz, and a 10 cm focal depth.

C. Image Quality Measurements

Image quality improvements due to coded excitation were quantified using SNR, contrast ratio (CR), and contrast-to-noise ratio (CNR). SNR was defined based on a previously reported spatiotemporal coherence technique where the contributions of noise and clutter are measured separately with spatial and temporal lag-one coherence [19]. SNR is therefore defined as the ratio of the power of the uncorrupted signal, P_s, and the power of the thermal noise, P_N, as given in (1):

$$\text{SNR} = 10\log_{10}\left(\frac{P_s}{P_N}\right) \tag{1}$$

The advantage of this measure of SNR is that stationary clutter is not included in the "signal" term which is the case with a typical normalized cross-correlation based measure of SNR, i.e., $\rho/(1-\rho)$. The signal powers are calculated based on spatial and temporal lag-one coherence measures computed within a region of interest (ROI) centered about the transmit focus of 10 cm (using the M-Mode data for this work). For more details about how this metric is calculated, see Vienneau *et al.* [19]. SNR gain between non-coded and coded excitation was calculated according to

$$\text{SNR}_{\text{gain}} = \text{SNR}_{\text{coded}} - \text{SNR}_{\text{non-coded}}. \tag{2}$$

Note that these measurements are computed on the channel data prior to clutter filtering or power Doppler processing. The SNR gain computed at this step is proportional to the gain in blood flow sensitivity.

Finally, measures of blood vessel detectability were computed using the *in vivo* transcranial power Doppler data. ROIs of approximately the same size and depth were manually selected inside (i) and outside (o) of blood vessels. Contrast ratio (CR) and contrast-to-noise ratio (CNR) were computed according to (3) and (4).

$$\text{CR} = 10\log_{10}\left(\frac{\mu_i}{\mu_o}\right) \tag{3}$$

$$\text{CNR} = 10\log_{10}\left(\frac{|\mu_i - \mu_o|}{\sqrt{\sigma_i^2 + \sigma_o^2}}\right) \tag{4}$$

We computed contrast ratio gain and CNR gain by subtracting the non-coded values from the coded values, similar to (2). These gains demonstrate improvements in blood flow visibility which also reflect an improvement in blood flow sensitivity.

TABLE I
IMAGE QUALITY IMPROVEMENTS

Code Length	SNR Gain	CNR Gain	CR Gain
13 bits	12.59 ± 0.22 dB	4.69 ± 5.15	13.15 ± 6.82
39 bits	14.98 ± 0.80 dB	4.48 ± 1.69	14.65 ± 5.20
65 bits	17.77 ± 1.05 dB	4.97 ± 4.18	22.53 ± 11.34

III. RESULTS

Fig. 1 shows an example B-Mode image in Subject 3 as a reference. The ROI delineated by the red box is region used for power Doppler processing (including the SVD filtering). The midbrain, part of the brain stem, is clearly visible in the B-Mode image as indicated by the arrow. This is an important landmark structure because there are many blood vessels surrounding the midbrain.

Transcranial power Doppler imaging results in Subject 3 with 13, 39, and 65 bit codes are shown in Figs. 2 and 3. Fig. 2 shows results using an IIR clutter filter. With this simple filter, virtually no blood flow is visible in the non-coded excitation images. With coded excitation, blood flow becomes apparent and visibility improves with longer codes. Qualitatively, it is evident that coded excitation effectively reduces the noise floor and increases the blood signal, thereby improving blood flow sensitivity. Also, particularly in the 65 bit coded excitation example, it is clear that the vessels that are visible are surrounding the midbrain.

In Fig. 3, more blood flow is visible for both the non-coded and coded excitation cases using the more advanced spatiotemporal SVD filter. Substantial improvements are again apparent with coded excitation. Qualitatively, the noise floor is still clearly reduced with coded excitation and much more blood flow is visible throughout. Quantitatively, the SNR, CNR, and CR are much higher with coded excitation and with increasing code length as indicated in the coded excitation panels in Fig. 3. The average SNR, CNR, and CR gains in all three subjects are shown in Table I. With a 65 bit code, SNR gains of nearly 18 dB are achieved, along with CNR gains of nearly 5 dB and CR gains of over 22 dB.

IV. CONCLUSION

We demonstrated dramatic improvements in image quality in transcranial power Doppler imaging in three healthy adult subjects using our coded excitation framework. The SNR gain from coded excitation reduced the noise floor and increased the blood flow signal, thereby improving blood flow visibility as evidenced by large increases in CNR and CR. These improvements in SNR, CNR, and CR translate to increased blood flow sensitivity. With our coded excitation technique, transcranial functional ultrasound neuroimaging may be feasible without contrast agents.

ACKNOWLEDGMENT

We acknowledge Vanderbilt University's Advanced Computing Center for Research and Education (ACCRE).

REFERENCES

[1] T. Deffieux, C. Demené, and M. Tanter, "Functional ultrasound imaging: A new imaging modality for neuroscience," *Neuroscience*, vol. 474, pp. 110–121, 2021.

[2] T. Deffieux, C. Demené, M. Pernot, and M. Tanter, "Functional ultrasound neuroimaging: a review of the preclinical and clinical state of the art," *Current Opinion in Neurobiology*, vol. 50, pp. 128–135, 2018.

[3] J. Baranger, C. Demené, A. Frerot, F. Faure, C. Delanoë, H. Serroune, A. Houdouin, J. Mairesse, V. Biran, O. Baud, and M. Tanter, "Bedside functional monitoring of the dynamic brain connectivity in human neonates," *Nature Communications*, vol. 12, no. 1080, 2021.

[4] M. Imbault, D. Chauvet, J.-L. Gennisson, L. Capelle, and M. Tanter, "Intraoperative functional ultrasound imaging of human brain activity," *Scientific Reports*, vol. 7, no. 7304, 2017.

[5] S. Soloukey, A. J. P. E. Vincent, D. D. Satoer, F. Mastik, M. Smits, C. M. F. Dirven, C. Strydis, J. G. Bosch, A. F. W. van der Steen, C. I. D. Zeeuw, S. K. E. Koekkoek, and P. Kruizinga, "Functional ultrasound (fus) during awake brain surgery: The clinical potential of intra-operative functional and vascular brain mapping," *Frontiers in Neuroscience*, vol. 13, no. 1384, 2020.

[6] G. Pinton, J. F. Aubry, E. Bossy, M. Muller, M. Pernot, and M. Tanter, "Attenuation, scattering, and absorption of ultrasound in the skull bone," *Medical Physics*, vol. 39, no. 1, pp. 299–307, 2012.

[7] K. K. Shung, R. A. Sigelmann, and J. M. Reid, "Scattering of ultrasound by blood," *IEEE Transactions on Biomedical Engineering*, vol. BME-23, no. 6, pp. 460–467, 1976.

[8] S. Bjærum, H. Torp, and K. Kristoffersen, "Clutter filter design for ultrasound color flow imaging," *IEEE Transactions on Ultrasonics, Ferroelectrics, and Frequency Control*, vol. 49, no. 2, pp. 204–216, 2002.

[9] A. Heimdal and H. Torp, "Ultrasound Doppler measurements of low velocity blood flow: limitations due to clutter signals from vibrating muscles," *IEEE Transactions on Ultrasonics, Ferroelectrics, and Frequency Control*, vol. 44, no. 4, pp. 873–881, 1997.

[10] J. Tierney, C. Coolbaugh, T. Towse, and B. Byram, "Adaptive clutter demodulation for non-contrast ultrasound perfusion imaging," *IEEE Transactions on Medical Imaging*, vol. 36, no. 9, pp. 1979–1991, 2017.

[11] J. Tierney, K. Walsh, H. Griffith, J. Baker, D. B. Brown, and B. Byram, "Combining slow flow techniques with adaptive demodulation for improved perfusion ultrasound imaging without contrast," *IEEE Transactions on Ultrasonics, Ferroelectrics, and Frequency Control*, vol. 66, no. 5, pp. 834–848, 2019.

[12] C. Demené, J. Robin, A. Dizeux, B. Heiles, M. Pernot, M. Tanter, and F. Perren, "Transcranial ultrafast ultrasound localization microscopy of brain vasculature in patients," *Nature Biomedical Engineering*, vol. 5, pp. 219–228, 2021.

[13] T. Misaridis and J. A. Jensen, "Use of modulated excitation signals in medical ultrasound. Part I: basic concepts and expected benefits," *IEEE Transactions on Ultrasonics, Ferroelectrics, and Frequency Control*, vol. 52, no. 2, pp. 177–191, 2005.

[14] R. Y. Chiao and X. Hao, "Coded excitation for diagnostic ultrasound: a system developer's perspective," *IEEE Transactions on Ultrasonics, Ferroelectrics and Frequency Control*, vol. 52, no. 2, pp. 160–170, 2005.

[15] E. Vienneau and B. Byram, "Compound Barker-coded excitation for increased signal-to-noise ratio and penetration depth in transcranial ultrasound imaging," *2020 IEEE International Ultrasonics Symposium (IUS)*, pp. 1–4, September 2020.

[16] E. P. Vienneau and B. C. Byram, "A coded excitation framework for increased signal-to-noise ratio of in vivo ultrasound power Doppler imaging," *Proceedings of SPIE 11602, Medical Imaging 2021: Ultrasonic Imaging and Tomography*, 116020P, February 2021.

[17] E. P. Vienneau and B. C. Byram, "Method and system using coded excitation with invertible skew-symmetric binary sequences and inverse filtering," WO2022/051238, September 4th, 2020.

[18] US Food and Drug Administration. (2019, June 27) Marketing clearance of diagnostic ultrasound systems and transducers: guidance for industry and Food and Drug Administration staff. [Online]. Available: https://www.fda.gov/media/71100/download

[19] E. P. Vienneau, K. A. Ozgun, and B. C. Byram, "Spatiotemporal coherence to quantify sources of image degradation in ultrasonic imaging," *IEEE Transactions on Ultrasonics, Ferroelectrics, and Frequency Control*, vol. 69, no. 4, pp. 1337–1352, 2022.